Annu. Rev. Fluid Mech. 1992. 24 : 205–33

ATMOSPHERIC TURBULENCE

John C. Wyngaard

Department of Meteorology, 508 Walker Building, The Pennsylvania State University, University Park, Pennsylvania 16802

KEY WORDS: atmospheric boundary layer, turbulence simulation, numerical simulation, flow measurements

1. INTRODUCTION

Atmospheric turbulence spans a huge range of scales. Turbulent eddies are important elements in the global circulation, in synoptic weather systems, in regional circulations, in severe storms, in clouds, in the atmospheric boundary layer, and in plant canopies. In its large-scale limit atmospheric turbulence approaches two dimensionality, while its smaller-scale forms are inherently three-dimensional. These are dynamically and structurally quite different varieties of turbulence (Tennekes 1978).

Three-dimensional turbulence occurs throughout the atmosphere. Well above the surface it appears locally and intermittently—in clouds, where it is generated by the energy released through condensation, and in clear air, due to instabilities associated with gravity waves and wind shear. I will focus on the atmospheric boundary layer, where three-dimensional turbulence occurs nearly continuously in space and time. There it transfers heat, momentum, and trace constituents between earth and atmosphere; diffuses pollutants; and carries the wind gusts that load structures, jostle aircraft passengers, move dunes, and erode soil.

Turbulence is a notoriously difficult subject. Generations of study have not revealed many of its inner secrets; as yet there is no generally accepted way to calculate its structure or its transport properties. Much of the motivation for research on atmospheric turbulence stems from interest in its effects, and making progress in such problems usually requires one to model certain key turbulence physics. Simulation is proving invaluable in generating improved turbulence models (Section 7).

In a review of a monograph on turbulent diffusion, Scorer (1980) wrote

0066–4189/92/0115–0205$02.00

> . . . because turbulence makes itself more complicated all the time so that no full description is possible, most theories are not theories about the turbulence at all, but about the consequences. . . . In the great outdoors we have, particularly in the atmosphere, an unending succession of different cases, whereas it is a characteristic of the models that they refer only to particular cases. One is always bound to wonder whether the models are relevant enough to be worth the bother. . . .

Hunt (1981) responded

> This approach is dismissed as useless by Professor Scorer . . . because nature is too complicated, he says, it cannot be codified . . . if we are to follow his advice and discuss nature eddy by eddy, how is the government inspector to make his decision and how are others to argue with him?

This exchange hints not only at the controversy that attends the modeling of atmospheric turbulence, but also at one of its important features—the large, persistent excursions about its statistical mean state, or what I call its high stochastic variability. This is important in a wide variety of applications. There are calls to include stochastic variability in air quality models (Weil 1985) and in the subgrid models used in large-eddy simulation (Section 7). I believe it is still useful to view Scorer's "unending succession of different cases" through simple, less ambitious models, however, and I do so here.

2. THE NATURE OF ATMOSPHERIC TURBULENCE

The turbulence in the atmospheric boundary layer is only part of a continuous spectrum of atmospheric motions. Certain conditions must be met in order to discuss its statistical properties in isolation from the larger-scale turbulence in which it is embedded. Lumley & Panofsky (1964) suggest that one such condition is that there be a gap in the spectrum. The results of Van der Hoven (1957), which show a minimum at periods of the order of one hour in the spectrum of wind speed near the ground, are widely cited as evidence of such a gap. It has become standard practice in boundary-layer meteorology to treat those fluctuations of periods less than about one hour as "turbulence" and to consider the slower fluctuations as part of the mean field.

In the daytime over land, the length scale ℓ of the flux-carrying eddies is of the order of the boundary-layer depth, say 1 km, and the velocity scale q is typically 1 m s^{-1}. The large-eddy Reynolds number $R_\ell = q\ell/\nu$ is of order 10^8, far larger than that in typical laboratory turbulence. The smallest, dissipative eddies scale with the Kolmogorov microscale $\eta = (\nu^3/\varepsilon)^{1/4}$. The dissipation rate per unit mass ε in any turbulent flow is of order q^3/ℓ (Tennekes & Lumley 1972), so $\eta \sim R_\ell^{-3/4}\ell \sim 10^{-3}$ m. The Taylor microscale λ, defined through $\varepsilon = \nu q^2/\lambda^2$, is 0.1 m for our

conditions. It typically marks the small-scale end of the $\kappa^{-5/3}$ Kolmogorov inertial subrange that appears at wavenumbers κ sufficiently distant from both the energy-containing and dissipative ranges.

Observations show an extensive inertial range in velocity spectra (Kaimal et al 1972, Young 1987, Chou & Yeh 1987). The corresponding Corrsin (1951) prediction for the temperature spectrum is confirmed at the larger-scale end of the inertial range, but a "bump" is seen just before the diffusive cutoff (Champagne et al 1977). Hill (1978a) has predicted such a bump, whose amplitude depends on the ratio of momentum and scalar diffusivities. This bump impacts electromagnetic wave propagation (Hill 1978b). Cospectra of stress and scalar flux fall faster than $\kappa^{-5/3}$ in the inertial range, consistent with an approach to local isotropy at larger wavenumbers. Inertial range spectral constants agree well with the values measured in laboratory turbulence (Champagne 1978, Andreas 1987).

In analyzing data from many different flows, including the atmospheric boundary layer, Champagne (1978) found that the high-wavenumber velocity spectral shape depends only on turbulence Reynolds number R_λ; the high-wavenumber end of the dissipative range becomes fuller with increasing R_λ. Antonia et al (1986) found evidence of anisotropy in the fine-structure data from moderate R_λ laboratory flows, with no strong indication of a decrease in this anisotropy in larger R_λ geophysical data. Brasseur (1991) has argued that local isotropy is, in principle, not possible unless the entire spectrum of scales is isotropic.

The notion of persistent local anisotropy in high R_λ turbulence merits continuing experimental examination. As discussed by Antonia et al (1986), this is a technically challenging problem. As R_λ increases, the fine-structure field becomes increasingly intermittent (Figure 1), increasing the difficulty of accurate, statistically reliable measurements (Section 3).

The three-dimensional spatial structure of the turbulent velocity field is needed in assessing the effects of wind loading on structures. Such information is relatively sparse, since it depends on the state of the boundary layer (Section 4) and is difficult to obtain experimentally (Section 3). Useful models of spatial structure have been made, however (e.g. Hunt et al 1988, Kristensen et al 1989). Further progress on modeling spatial structure could come through numerical simulation (Section 7).

The larger length scales and smaller velocity scales of atmospheric turbulence, compared to typical engineering turbulence, imply that buoyancy effects are apt to be more important in the atmosphere. In the Boussinesq approximation, turbulent buoyancy forces per unit mass are of order $\beta\delta T_v$, where $\beta = g/T$, the acceleration of gravity/mean temperature and δT_v is a virtual temperature deviation from the mean. [It is conventional (e.g. Lumley & Panofsky 1964) to treat moist air as a perfect gas with a gas

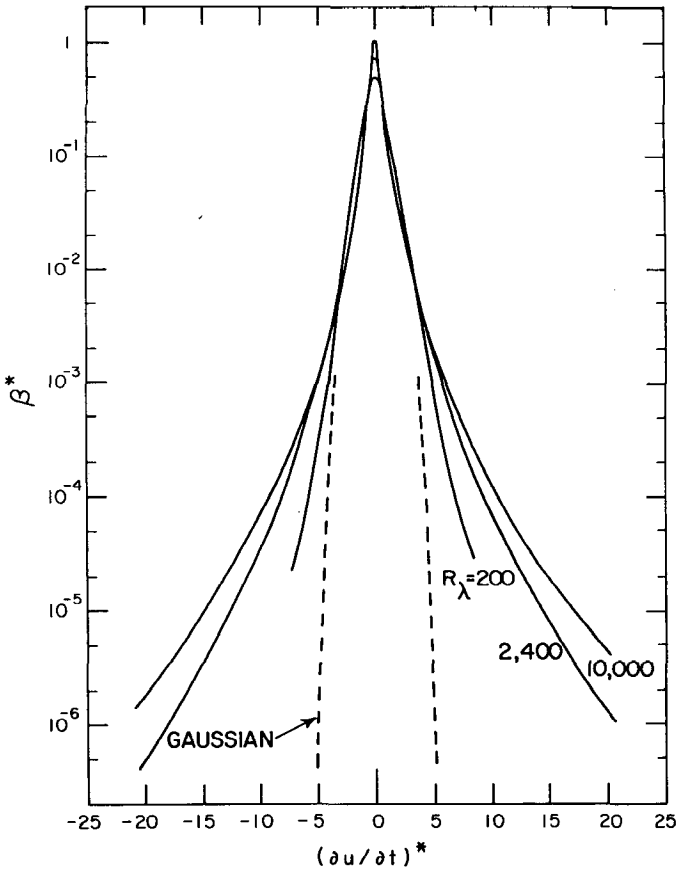

Figure 1 Probability densities of the streamwise velocity derivative (made dimensionless with its rms value) measured at various turbulent Reynolds numbers. As R_λ increases the probability of very large and near-zero values increases, reflecting the increasing intermittency of fine structure.

constant of dry air but having a "virtual" temperature T_v—that temperature which dry air would have to have in order to produce the actual density at the actual pressure.] Turbulent inertia forces per unit mass are of order q^2/ℓ. Their ratio, $\beta\delta T_v \ell/q^2$, is a turbulence Richardson number. In daytime turbulence with $q = 1$ m s^{-1} and $\ell = 10^3$ m, this is $\mathcal{O}(1)$ for $\delta T_v \sim 0.03$ K. Since typical temperature fluctuation levels are at least this large, truly neutral (i.e. unaffected by buoyancy) atmospheric turbulence is rare. Turbulence Mach numbers are typically small, however,

so that the changes in density due to dynamic effects are negligible and the atmosphere can be regarded as otherwise incompressible.

Daytime turbulence is readily sustained by the buoyancy forces that result from surface heating and evaporation. Convection fills the space available so $\ell \sim z_i$, the distance to the first inversion base. At night, radiative cooling of the earth's surface causes a positive vertical gradient of potential temperature $\theta_{,3}$ near the surface. (In order to account for the height variation of temperature in an adiabatic atmosphere, we use a potential temperature $\theta = \text{constant} \times T/(P)^{R/c_p}$, which is conserved in an isentropic change.) Vertical displacements ℓ produce temperature fluctuations of order $-\theta_{,3}\ell$ and a restoring buoyancy force of order $\beta\theta_{,3}\ell$. The largest eddies surviving this energy drain to buoyancy are those having inertia forces at least as large, so that $q^2/\ell \geq \beta\theta_{,3}\ell$. In an equilibrium, stably stratified boundary layer this implies a maximum eddy size $\ell \sim (q^2/\beta\theta_{,3})^{1/2}$. These simple arguments are consistent with observations and with numerical simulation results (Section 7).

Both unstable and stable stratification can also be generated by heat transfer at the boundary-layer top. Lilly (1968) proposed that cloud-top cooling was the chief source of turbulence in the stratus-topped boundary layer, a notion that has subsequently been explored in detail by Deardorff (1980), Moeng (1986), Duynkerke & Driedonks (1987), Chen & Cotton (1987), Hanson (1987), and Curry et al (1988). Analogously, entrainment of less-dense air from above is an alternative to surface cooling as a mechanism for generating a stably stratified boundary layer.

Mean wind shear is the sole source of turbulent kinetic energy in the neutral and stably stratified boundary layers, and can also be significant in the convective case. Additional turbulence production mechanisms are associated with hilly terrain, the circulations around and phase change within clouds, and spatial variations in surface roughness.

As the surface energy budget over land changes in response to the evolving radiative flux at the surface, the surface heat flux and the stratification of the boundary layer change as well. A characteristic large-eddy time of the turbulence, $\tau_t \sim \ell/q$, can be much smaller than the time scale τ_b of these evolving boundary conditions. For example, in the daytime with $\ell = 10^3$ m and $q = 1$ m s^{-1}, $\tau_t \sim 10^3$ s; if τ_b is a few hours, then $\tau_t \ll \tau_b$. In such cases the turbulence can be assumed to be quasi-steady.

In a coordinate system fixed to the earth, the momentum equation contains a Coriolis term proportional to the vector product of the earth's rotation rate Ω and the turbulent velocity. The ratio of turbulent Coriolis and inertia forces is of order $\Omega\tau_t = \text{Ro}^{-1}$, where Ro is a turbulence Rossby number. Ro is $\mathcal{O}(1)$ in a neutral boundary layer, so one expects some structural consequences of turbulent Coriolis forces there (e.g. a depen-

dence of turbulence properties on latitude and mean wind direction); this is confirmed by the numerical simulations of Coleman et al (1990a). Since neutral cases are rare, and since Ro is substantially larger in typical convective and stably stratified cases, turbulent Coriolis forces can usually be neglected in the boundary layer.

The turbulent component of radiative flux divergence appears in the equation for fluctuating temperature. The time scale of this radiative term is usually large compared to the time scale ℓ/q of the leading terms, so that the direct effects of radiative flux divergence on the turbulence can be neglected.

The boundary layer evolves in the downstream direction as it responds to spatial variations in surface texture. If the scale of these surface variations is L, then following the mean motion U the embedded turbulence sees boundary conditions changing with time scale $\tau_b \sim L/U$. Again, if $\tau_t \sim \ell/q \ll L/U$, the turbulence will see these changes as slow. Thus, we can consider the turbulence to be locally homogeneous if $\ell U/(qL) \ll 1$.

3. MEASURING ATMOSPHERIC TURBULENCE

Until recently most of our detailed knowledge of the structure of turbulent flows came from direct measurements, but turbulence simulation is now also a frontline tool (Reynolds 1990). Certain turbulence properties—the pressure and vorticity fields, for example—have always been difficult to measure (Corrsin 1963). Atmospheric turbulence offers little relief; its larger spatial scale makes it easier to resolve fine structure, but complicates measurements of energy-containing structure. Measurements over the atmospheric boundary layer depth can require aircraft platforms, and measurements that require multiple probes have been all but impossible. Remote sensors such as Doppler radars are now being used to produce turbulence statistics (e.g. Frisch et al 1989).

The high stochastic variability of atmospheric turbulence leads to large scatter in time averages. Our formal descriptions of turbulence typically use ensemble averages, but time averages are more convenient and an acceptable substitute in quasi-steady flows. The time required for the convergence of a time average to the ensemble average is well known. If $f(t)$ is a stationary, random function of time with integral scale τ, σ^2 the ensemble variance of the time average f_T (for averaging period T) about the ensemble average $\overline{f}$, and $\overline{f'^2}$ the ensemble variance of f about $\overline{f}$, then one has (Lumley & Panofsky 1964)

$$\frac{T}{\tau} = \frac{2\overline{f'^2}}{\sigma^2}. \qquad (1)$$

If one wishes to estimate an ensemble-average velocity variance $\overline{u^2}$, say, through a time average, (1) shows that

$$\frac{T}{\tau} \sim \frac{2(K-1)(\overline{u^2})^2}{\sigma^2}, \tag{2}$$

where $K = \overline{u^4}/(\overline{u^2})^2$ is the kurtosis of u. In view of the diurnal cycle and other nonstationary influences, the longest feasible averaging time T is of the order of one hour. If we use the Gaussian value of $K = 3$, take $\tau \sim \ell/U_1$ with U_1, the mean wind speed that advects the turbulence past the probe, of 5 m s^{-1}, and use $\ell = 0.3z_i$ (Lenschow & Stankov 1986) with $z_i =$ 1000 m, then Equation (2) shows that $\sigma \sim \overline{u^2}/4$. Thus, the uncertainty in $\overline{u^2}$ estimated through one hour averages is about 1/4 of $\overline{u^2}$ itself. Since the required averaging time varies as σ^{-2}, reducing the expected measurement scatter to the level attainable in engineering flows—10%, say—can require very long averaging times (or flight legs) in the atmosphere. Equation (1) indicates that fluxes have even more scatter than variances, since their $\overline{f'^2}$ values are relatively larger.

Experience confirms these predictions (Wyngaard 1973, Lenschow & Stankov 1986). What Mahrt (1989) calls "global intermittency"—a large-scale inhomogeneity, or patchiness, of the energy-containing turbulence—can make it particularly difficult to calculate reliable statistics near the boundary-layer top (Atlas et al 1986) and under stable stratification (Mahrt & Gamage 1987). The tendency toward large scatter limits the utility of direct measurements in discriminating among competing models (Lenschow et al 1980, Weil 1985). It has also provided some of the incentive to use simulation instead of direct measurements (Section 7).

Historically, turbulence researchers have calibrated their probes and their mounts in test flows to account for the myriad of factors influencing their performance in turbulence (Corrsin 1963). Atmospheric researchers can rarely do this; their instrument platforms (ships, aircraft, towers, booms) are usually too large to fit into wind tunnels. Thus, their instrument calibrations usually ignore the flow distortion due to the measurement platform. Wieringa (1980) attempted to correct turbulence statistics from the 1968 Kansas field program for flow distortion caused by the instrument tower. This had been a neglected problem in micrometeorology, although attention had been given to the effects of flow distortion on mean wind measurements (Wucknitz 1980). His corrections were challenged by Wyngaard et al (1982), but their analysis did confirm that flow-distortion effects on turbulence can be severe. It seems possible that some of the long-running disputes about profile forms and universal constants in surface-layer micrometeorology (Yaglom 1977) were fed in part by the systematic errors caused by flow distortion.

Turbulence measurements from aircraft are also vulnerable to errors from flow distortion. Reynolds shearing stress measured from aircraft nose booms can be degraded by the fuselage-induced flow distortion (Wyngaard et al 1985), and compressibility effects at aircraft speeds (Mach number ~ 0.3) can interact with turbulent velocity and temperature fluctuations to create "false fluctuations" of a conservative species density and errors in its measured flux (Wyngaard 1988).

4. SIMILARITY STRUCTURE

Figure 2 depicts the convective boundary layer—the common daytime state over land, driven by the temperature flux at the surface and, to a lesser extent, the moisture flux. It also exists commonly over the sea, where the moisture flux dominates. An inversion typically serves as its top. It can be divided into three regions (Deardorff 1979), as shown in Figure 3: the surface layer, the mixed layer, and the interfacial layer.

Figure 4 depicts the stably stratified boundary layer with surface cooling. It occurs under clear skies at night, when the radiative loss at the surface causes a stable lapse rate that diffuses upwards with time; it also occurs in warm-air advection over a cooler surface. It sets its own depth at the level where turbulence is extinguished by the stratification. A variant of this case has negligible surface buoyancy flux, with the stable stratification generated by heating from above. This can be due to the presence of a low inversion, for example, whose entrainment by the turbulence below leads

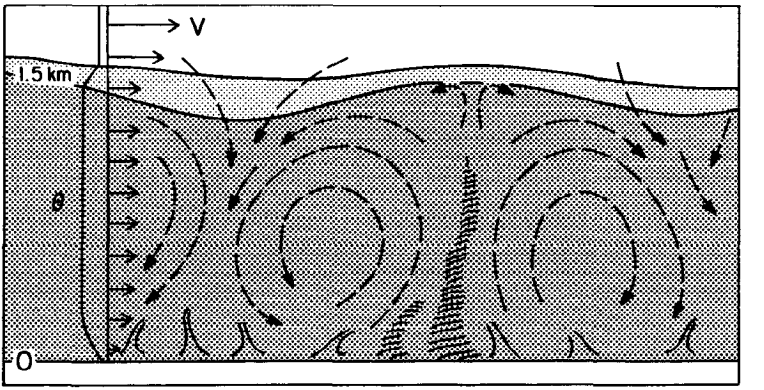

Figure 2 A schematic of the convective boundary layer showing its large eddies, convective plumes, flat wind profile, and the capping inversion layer.

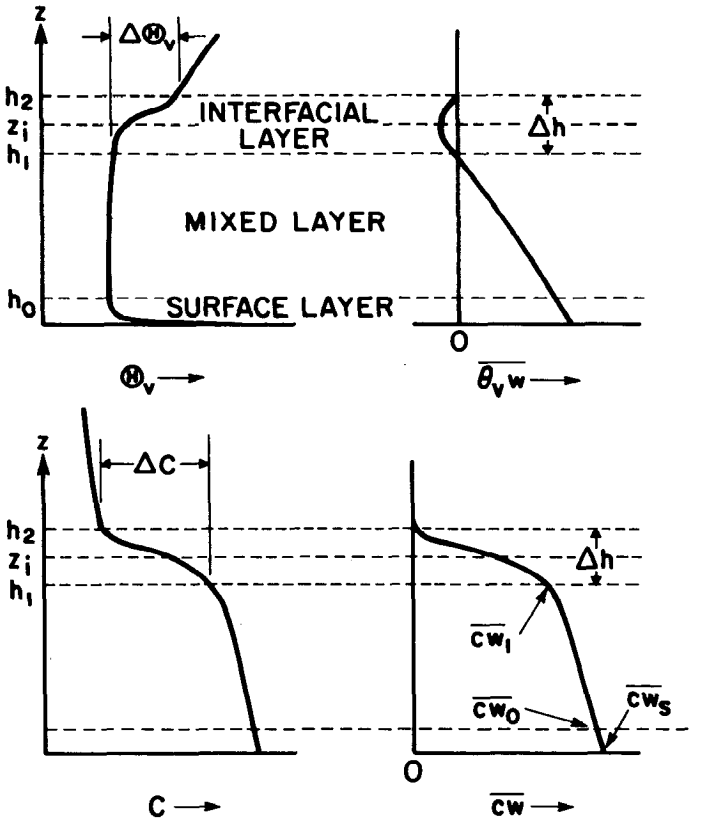

Figure 3 Top panel: Deardroff's (1979) schematic of the convective boundary layer. Left, the profile of mean virtual potential temperature; right, the profile of the virtual temperature flux, whose zero crossings define the interfacial layer. Bottom: The profiles of the mean value (*left*) and vertical flux (*right*) of a conservative scalar constituent.

to a downward heat flux. We will call this the inversion-capped neutral layer.

The lowest portion (10%, say) of the boundary layer, where the turbulent fluxes are little changed from their surface values, is called the surface layer. Being the most accessible to measurement, it is the best understood. The Monin-Obukhov similarity hypothesis holds that above a statistically homogeneous surface—beyond the molecular sublayer, but within the "constant-flux" layer—the structure of the energy-containing turbulence depends only on distance from the surface (traditionally called z), the Boussinesq buoyancy parameter $\beta = g/T$, the surface temperature

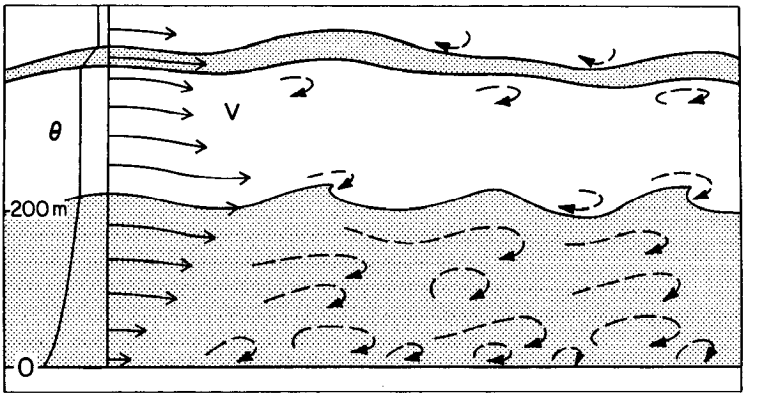

Figure 4 A schematic of the stably stratified boundary layer showing its shallow depth, small eddies, and large wind shear.

flux Q_0, and the friction velocity (the square root of the kinematic surface stress) u_*. Statistics made dimensionless with scales z (length), u_* (velocity), and $T_* = -Q_0/u_*$ (temperature) are hypothesized to be universal functions of the stability parameter z/L, where $L = -u_*^3/k\beta Q_0$ is the Monin-Obukhov length. (The von Karman constant k is traditionally included.)

For large instabilities—negative z/L values on the order of 1—some surface-layer statistics show signs of following the predictions of free convection theory, despite the presence of mean wind shear and surface stress. Tennekes (1970) coined the term "local free convection" to describe this regime at the outer edge of the unstable surface layer. It can be interpreted physically as the result of the increasing influence of turbulent buoyancy forces with height. At some height the convective turbulence so dominates the mechanical turbulence that u_* drops out of the governing parameter group. The scales become $u_f = (\beta Q_0 z)^{1/3}$ for velocity, $T_f = Q_0/u_f$ for temperature, and z for length; the local turbulent Richardson number $\beta T_f z/u_f^2$ is independent of z. In the local free convection limit we expect $\overline{u_3^2} \sim u_f^2$, $\overline{\theta^2} \sim T_f^2$—or equivalently, $\overline{u_3^2}/u_*^2 \sim (z/L)^{2/3}$, $\overline{\theta^2}/T_*^2 \sim (z/L)^{-2/3}$. These predictions are borne out well by observations (Panofsky & Dutton 1984).

Measurements also show an asymptote under very stable conditions—at $z/L \sim 1$. The physical interpretation is that at sufficient height the loss of turbulent kinetic energy to buoyancy limits the size of the largest eddies. They can no longer be as large as the distance to the surface, so z loses its significance and drops out of the governing parameter group. The scales become u_*, T_*, and L; the mean wind gradient $\partial U/\partial z$, for example, should

approach u_*/L—or equivalently, $\phi_m = (kz/u_*)\partial U/\partial z \sim z/L$. This behavior is observed (Panofsky & Dutton 1984).

The M-O hypothesis has brought order to surface-layer data. It is useful even at sites that are less than ideal (Brutsaert & Sugith 1990). It does have some deficiencies; for example, it does not admit the influence of the large convective eddies. The horizontal turbulent wind field in the convective surface layer seems to scale with the convective velocity scale $w_* = (\beta Q_0 z_i)^{1/3}$ rather than u_* (Panofsky & Dutton 1984). One can speculate that this mechanism causes other deviations from M-O similarity. Another failure concerns scalar statistics. Hill (1989) shows that the M-O hypothesis implies that the correlation coefficient between any two conservative scalars transferred through the surface (for example, temperature and water vapor mixing ratio) is 1.0 in magnitude. Although the correlation coefficient is often observed to be large, this prediction is strictly incorrect, evidently because the M-O hypothesis neglects surface-transfer physics of scalars. Kader & Yaglom (1990) suggest that some other apparent deviations from M-O similarity can be accounted for by generalizing it to include different horizontal and vertical length scales. Hogstrom (1990) contends that surface roughness length and boundary-layer depth affect neutral surface layer structure.

The mid portions of the convective boundary layer are called the "mixed layer" (Figure 3) because of the strong mixing characteristics of its buoyancy-driven turbulence. Deardorff (1970) suggested that the governing parameters for turbulence in this layer are β, z, z_i, and Q_0. In this "mixed-layer scaling" hypothesis, statistics made dimensionless with w_*, z, and a temperature scale $\theta_* = Q_0/w_*$ are universal functions of z/z_i. For example, temperature variance $\overline{\theta^2}$ is hypothesized to vary as $\theta_*^2 f(z/z_i)$, where f is a function to be determined. Near the bottom of the mixed layer these functions often agree with the local free convection prediction. For example, for temperature and vertical velocity variances we have $\overline{\theta^2} \sim T_f^2 \sim \theta_*^2 (z/z_i)^{-2/3}$, $\overline{u_3^2} \sim u_f^2 \sim w_*^2 (z/z_i)^{2/3}$, which are observed (Panofsky & Dutton 1984).

As with M-O similarity, the detailed and systematic measurements necessary to assess the range of validity of mixed-layer scaling have not been done. Kustas & Brutsaert (1987) found that over complex terrain the effects of mechanical turbulence due to the terrain could not be neglected, but others (e.g. Huyuh et al 1990) have found that over moderate terrain under sufficiently convective conditions, mixed-layer scaling did continue to hold. The entrainment at the mixed-layer top influences turbulence statistics—particularly those of scalars—well within the mixed layer (Kaimal et al 1976, Caughey 1982, Huyuh et al 1990). Temperature fluctuations, for example, typically follow the mixed-layer prediction only until

mid-layer, where they begin to increase with height because of entrainment-induced fluctuations; water vapor fluctuations often depart sooner (Figure 5).

One way to account for entrainment effects on scalars is the "top-down, bottom-up" decomposition of Wyngaard & Brost (1984). They suggested that any conservative scalar field c can be written as the sum of a "top-down" part c_t due to the entrainment flux and a "bottom-up" part c_b due to the surface flux. Mixed-layer scaling deals only with the latter. An obvious hypothesis is that c_t scales with the flux $\overline{cw}_1$ at mixed-layer top (Figure 3), so that $\overline{c_t^2} \sim (\overline{cw}_1/w_*)^2 g(z/z_i)$. The top-down function g can differ from the bottom-up function f. Moeng & Wyngaard (1984) estimated some of the top-down scaling functions through large-eddy simulation. They found that the c_t and c_b fields are correlated, so that the full variance is $\overline{c^2} = \overline{c_b^2} + 2\overline{c_b c_t} + \overline{c_t^2}$. Fairall (1987) used this scaling hypothesis to predict the behavior of the refractive index structure parameter in the convective boundary layer.

I know of no measurements in a truly neutral boundary layer—one with zero buoyancy flux throughout. Rarely are adequate time and inversion-free depth available for its development to a quasi-equilibrium state. The stably stratified case with surface buoyancy flux (Figure 4) has been documented (Caughey et al 1979, Nieuwstadt 1984, Lenschow et al 1988)

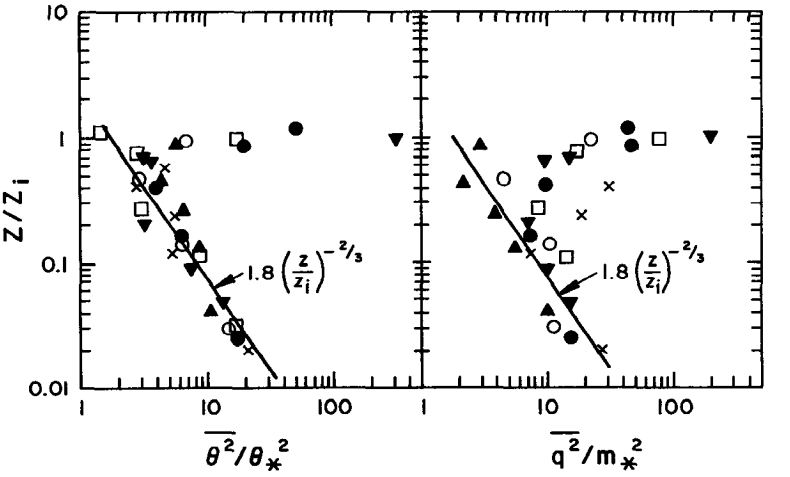

Figure 5 Vertical profiles of the variances of temperature (*left*) and water vapor mixing ratio (*right*) in a convective boundary layer (Lenschow et al 1980). They follow mixed-layer scaling at lower levels but show large departures higher up due to the effects of entrainment at the capping inversion.

as has, to a lesser extent, the inversion-capped neutral layer (Brost et al 1982, Duynkerke & Driedonks 1988). Nieuwstadt (1984) has proposed a local similarity theory for the former. He suggests that the appropriate scales are based on the local kinematic shear stress and temperature flux. These define a local M-O length L_ℓ. He hypothesizes that in analogy to M-O similarity, turbulence statistics made dimensionless with the "local" u_* and T_* are universal functions of the dimensionless height z/L_ℓ. As a closure hypothesis, he suggests that the local turbulence Richardson number approaches a limiting constant. These notions have recently received support through turbulence simulation (Section 7).

5. TURBULENT FLUXES

Turbulence is important in meteorological modeling (e.g. numerical weather prediction) because it carries large fluxes—far larger than those due to molecular diffusion. Within the surface layer, for example, the kinematic momentum fluxes due to molecular viscosity and turbulence are $\nu\partial U_1/\partial x_3$ and $\overline{u_1 u_3}$, respectively, and scale as $\nu u_*/kz$ and u_*^2; for $u_* = 0.3$ m s^{-1} and $kz = 3$ m their ratio is 10^{-5}.

A surface flux stems from a difference in the surface and atmospheric values of a property. The flux at the boundary-layer top vanishes if the turbulence does, but intermittent free-stream turbulence and clouds can support a nonzero flux there. The flux profile in between depends on the nature of the mean balance equation for the quantity and on the properties of the turbulence.

The flux profile can sometimes be deduced from the mean conservation equation, using only weak assumptions about the turbulence. Consider the simplest case where the mean of a conservative scalar constituent changes with time due to flux divergence,

$$\frac{\partial C}{\partial t} + \frac{\partial \overline{cw}}{\partial z} = 0. \tag{3}$$

If the flow is quasi-steady, $\partial C/\partial z$ does not change with time. This can happen with potential temperature in a mixed layer near midday; the layer warms but the flux and mean gradient do not change. (We must treat the interfacial layer separately, for its changes can be of the opposite sense when the convective boundary layer deepens due to entrainment and the interfacial layer rises. The temperature there decreases with time, for example.) This can also occur in a stable boundary layer at night if the flux and mean temperature gradient remain constant as temperature falls, as can occur with a constant surface cooling rate (Derbyshire 1990). It can

occur for trace constituents as well. Equation (3) then says that $\partial C/\partial t$ is independent of height, so the $\overline{cw}$ profile is linear; it can be written as

$$\overline{cw} = \overline{cw}(0) + [\overline{cw}(h_1) - \overline{cw}(0)]\frac{z}{h_1}. \tag{4}$$

In a mixed layer or an inversion-capped neutral layer, entrainment in the presence of a scalar gradient maintains a nonzero value of $\overline{cw}(h_1)$, the flux at the top (Figure 3).

As another example, consider a steady mean balance between height-dependent horizontal advection and flux divergence:

$$U(z)\frac{\partial C}{\partial x} + \frac{\partial \overline{cw}}{\partial z} = 0. \tag{5}$$

This can hold for potential temperature in the stably stratified boundary layer with warm-air advection over a colder surface, and in the convective mixed layer formed by cold-air advection over a warmer surface. There are analogous situations for trace constituents. Again, a weak closure hypothesis—that x-independence of the flux implies x-independence of the mean gradient—allows us to solve for the flux profile. It can be written

$$\overline{cw} = \frac{\overline{cw}(h_1)}{\langle U \rangle h_1}\int_0^z U(z')\,dz' + \overline{cw}(0), \tag{6}$$

where $\langle U \rangle$ is the layer-averaged U.

Another common situation is a steady balance between vertical advection and flux divergence:

$$W(z)\frac{\partial C}{\partial z} + \frac{\partial \overline{cw}}{\partial z} = 0. \tag{7}$$

This occurs in the mixed layer over the sea, where drying (or cooling) by subsidence W balances moistening (or heating) due to the divergence of the flux due to evaporation (or surface heat transfer). In contrast with the previous two examples, where a similarity assumption about the turbulence allowed us to eliminate the mean gradient from the mean conservation equation and solve for the flux profile, here we require a more specific closure statement—e.g. a relation between $\overline{cw}$ and $\partial C/\partial z$—in order to yield the flux profile.

For mean horizontal momentum, the simplest balance occurs under steady, horizontally homogeneous conditions:

$$\frac{\partial \overline{u_1 u_3}}{\partial x_3} = f(U_2 - U_{2g}), \tag{8}$$

$$\frac{\partial \overline{u_2 u_3}}{\partial x_3} = f(U_{1g} - U_1). \tag{9}$$

The mean horizontal pressure gradient (fU_{2g}, $-fU_{1g}$) is determined hydrostatically by the mean temperature field. In the absence of horizontal gradients of mean temperature (the barotropic case) this pressure gradient is independent of x_3. Let us see whether the turbulence might be sufficiently diffusive to also maintain U_1 and U_2 independent of x_3 above the surface layer, so that (8) and (9) can yield linear flux profiles. If mean wind shear and stress are related through an eddy viscosity $K \sim q\ell$, we can integrate that stress-shear relation to find an expression for the mean velocity change δU_i across a layer of depth h:

$$\frac{\delta U_i}{u_*} \sim \frac{\langle \overline{u_i u_3} \rangle}{q u_*} \frac{h}{\ell}, \qquad i = 1, 2 \tag{10}$$

where the brackets denote a representative value for the layer. If the stratification is stable, $q^2 \sim u_*^2 \sim \langle \overline{u_i u_3} \rangle$, $\ell < h$, so $\delta U_i / u_* > 1$. This says the mean wind shear can be large. In a strongly convective layer, however, $q^2 \sim w_*^2 \gg u_*^2$, $\ell \sim h$, so $\delta U_i / u_* < 1$ and the mean wind shear can be small. We conclude that only in the barotropic, convective boundary layer would we expect to approach height-independence of both the mean pressure gradient and the Coriolis term in (8) and (9) and, hence, approach linear stress profiles. An interesting special case is the baroclinic (x_3-varying pressure gradient) case with strong convection, where the wind profile can approach x_3-independence so the stress profile curves strongly to balance the variable pressure gradient.

The flux at the top of a mixed layer (Figure 3) or an inversion-capped neutral layer can be related to the entrainment rate and the change in mean quantities across the interfacial layer. Lilly (1968) showed that in the limit of small interfacial layer thickness the entrainment flux of a scalar is

$$\overline{cw}(h_1) = -w_e \Delta C. \tag{11}$$

Here $w_e = dh_1/dt - U_3(h_1)$ is the entrainment velocity—the net rate of change of layer depth with time, accounting for the mean vertical velocity at the planetary boundary layer (PBL) top, and $\Delta C = C(h_2) - C(h_1)$ is the mean change across the interfacial layer. Deardorff (1973) extended this to momentum flux:

$$\overline{u_i u_3}(h_1) = -w_e \Delta U_i, \qquad i = 1, 2. \tag{12}$$

The interfacial layer can be quite thick [20–60% of the mixed-layer depth, according to Deardorff (1979)]. The entrainment relations (11) and (12)

are then only approximate, due to the effect of terms neglected in their derivation.

The entrainment velocity w_e is quite important in boundary-layer modeling. It is typically one to two orders of magnitude smaller than the convective velocity w_*, and one order smaller than the friction velocity u_*. It is difficult to measure in the field directly through its definition $dz_i/dt - W(h_1)$, since these quantities are usually of the same size. Attempts have been made to calculate it through models of interfacial layer dynamics (Tennekes 1975, Zilitinkevich 1975, Tennekes & Driedonks 1981), but no definitive theory has emerged. Clearly w_e depends on the structure of the underlying boundary layer as well as the interfacial layer.

Given conditions at the surface and in the free atmosphere, the profile of a flux through the boundary layer can be determined by an entrainment condition (11) or (12), its counterpart for the surface layer (a drag law), plus a closure for the flux within the boundary layer. The profile need not be monotone; stress profiles, in particular, can have mid-layer extrema.

6. SECOND-MOMENT BUDGETS

Some insight into closures for atmospheric turbulence can be gained from the Reynolds equations for variances and for fluxes. The equation for turbulent velocity covariance $\overline{u_i u_k}$ in horizontally homogeneous atmospheric turbulence can be written

$$\frac{\partial \overline{u_i u_k}}{\partial t} = -\left(\overline{u_i u_j}\frac{\partial U_k}{\partial x_j} + \overline{u_k u_j}\frac{\partial U_i}{\partial x_j}\right) - \frac{\partial \overline{u_i u_k u_j}}{\partial x_j} - \frac{1}{\rho_0}\left(\overline{u_k \frac{\partial p}{\partial x_i}} + \overline{u_i \frac{\partial p}{\partial x_k}}\right)$$

$$-(\beta_i \overline{\theta u_k} + \beta_k \overline{\theta u_i}) - \frac{2}{3}\delta_{ik}\varepsilon, \quad (13)$$

where $\beta_i = (0, 0, -\beta)$ is the buoyancy vector. The terms on the right side represent, in order, shear production, turbulent transport, pressure interaction, buoyant production, and viscous dissipation. With the same approximations, the equation for the scalar flux $\overline{cu_i}$ is

$$\frac{\partial \overline{cu_i}}{\partial t} = -\left(\overline{u_i u_j}\frac{\partial C}{\partial x_j} + \overline{cu_j}\frac{\partial U_i}{\partial x_j}\right) - \frac{\partial \overline{u_i u_j c}}{\partial x_j} - \frac{1}{\rho_0}\overline{c\frac{\partial p}{\partial x_i}} - \beta_i \overline{c\theta}. \quad (14)$$

Here the terms on the right are gradient production, turbulent transport, pressure interaction, and buoyant production. We have neglected the small Coriolis terms and used the isotropic form for the molecular terms.

Equations (13) and (14), being the basis of the second-order-closure

modeling technique, have been studied in the surface layer and within the boundary layer as well.

Under quasi-steady, locally homogeneous conditions in the surface layer, and with the x_1-axis aligned with the surface stress, (13) yields the balance of turbulent kinetic energy $\overline{u_i u_i}/2$:

$$0 = -\overline{u_1 u_3}\frac{\partial U_1}{\partial x_3} - \frac{\partial}{\partial x_3}\frac{\overline{u_i u_i u_3}}{2} - \frac{1}{\rho_0}\frac{\partial}{\partial x_3}\overline{pu_3} + \beta\overline{\theta u_3} - \varepsilon. \tag{15}$$

Micrometeorologists typically nondimensionalize the energy budget (15) with u_* and kz and interpret the results through M-O similarity. Since $\overline{u_1 u_3}$ and $\overline{\theta u_3}$ are essentially equal to their surface values $-u_*^2$ and Q_0, the nondimensional shear and buoyant production terms in (15) become simply

$$\frac{kz}{u_*^3}\left(-\overline{u_1 u_3}\frac{\partial U_1}{\partial x_3}\right) = \phi_m, \qquad \frac{kz}{u_*^3}\beta\overline{\theta u_3} = -\frac{z}{L}; \tag{16}$$

so there is little uncertainty in these terms. Of the remaining terms in (15) all but the pressure transport have been measured, allowing it to be inferred from the budget imbalance. [Attempts to measure the pressure transport have been made (McBean & Elliot 1975, Dobson 1980) and renewed recently (S. Oncley of NCAR, personal communication)]. Figure 6 sketches the behavior of the budget under convective conditions as deduced from studied summarized by Hogstrom (1990). Significant features include the large gain from pressure transport and the large loss to turbulent transport (through export to levels above). Under stable conditions the budget is generally agreed to be essentially a local balance between shear production and the loss to dissipation and buoyancy.

With the same approximations, the budgets of shear stress and vertical scalar flux in the constant-flux layer can be written from (13) and (14) as

$$0 \simeq \frac{\partial \overline{u_1 u_3}}{\partial t} = -\overline{u_3^2}\frac{\partial U_1}{\partial x_3} - \frac{\partial \overline{u_3^3 u_1}}{\partial x_3} - \frac{1}{\rho_0}\left(\overline{u_1\frac{\partial p}{\partial x_3}} + \overline{u_3\frac{\partial p}{\partial x_1}}\right) + \beta\overline{\theta u_1}, \tag{17}$$

$$0 \simeq \frac{\partial \overline{cu_3}}{\partial t} = -\overline{u_3^2}\frac{\partial C}{\partial x_3} - \frac{\partial \overline{u_3^2 c}}{\partial x_3} - \frac{1}{\rho_0}\overline{c\frac{\partial p}{\partial x_3}} + \beta\overline{c\theta}. \tag{18}$$

In each case the terms on the right side represent gradient production, turbulent transport, pressure, and buoyancy effects, respectively.

Measurements of (17) and (18) in the surface layer (Wyngaard et al 1971) show two important features. First, the directly measurable terms—gradient production, turbulent transport, and buoyancy—have a large imbalance that is attributable to pressure destruction. Second, even under

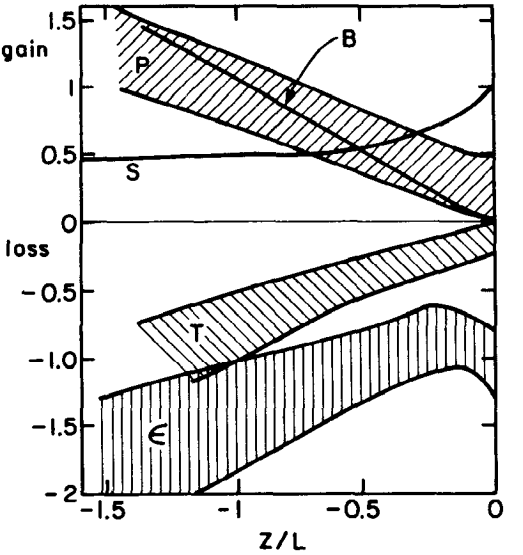

Figure 6 The budget of turbulent kinetic energy in the unstable surface layer. The shaded areas represent the spread of measurements from experiments summarized by Hogstrom (1990). B represents buoyant production; P, pressure transport; S, shear production; T, turbulent transport; and ε, viscous dissipation.

unstable conditions the turbulent transport is negligible. This means that to first approximation the stress and scalar flux budgets are in local balance, being produced by gradient production and buoyancy at the rate they are destroyed by pressure effects. This is quite remarkable; given the strong, vertically coherent updrafts in the unstable surface layer, one might have expected to find strong transport effects in these budgets—as there are, for example, in the turbulent kinetic energy budget. One result is that simple models based on the stress and heat flux equations have been quite successful in calculating the structure of the surface layer (Lewellen & Teske 1973, Mellor 1973). Such models either neglect turbulent transport or model it as a gradient diffusion process; the latter tends to be incorrect in this case (Wyngaard 1973, Moeng & Wyngaard 1989) but is not a serious error because of its small magnitude in the stress and scalar flux equations. They also represent the pressure term with Rotta's (1951) "return-to-isotropy" model, which for $\overline{u_1 u_3}$ and $\overline{cu_3}$ says

$$\frac{1}{\rho_0}\left(\overline{u_1 \frac{\partial p}{\partial x_3}} + \overline{u_3 \frac{\partial p}{\partial x_1}}\right) \sim \frac{\overline{u_1 u_3}}{\tau_1}, \tag{19}$$

$$\frac{1}{\rho_0} c \overline{\frac{\partial p}{\partial x_3}} \sim \frac{\overline{cu_3}}{\tau_2}, \tag{20}$$

the τ_i being turbulent time scales. Using this in models of (17) and (18) allows one to reproduce the observed mean wind and temperature gradients quite accurately. These simple models can also reproduce the effects of stability on the mean and turbulence profiles in the surface layer.

The broad outlines of the turbulent kinetic energy budget in the mixed layer are now evident from a combination of aircraft, tethered-balloon, and tall tower measurements (Kaimal et al 1976, Lenschow 1979, Caughey & Wyngaard 1979, Lenschow et al 1980, Caughey 1982). Figure 7 sketches its behavior. The principal turbulent kinetic energy source is buoyant production, the principal loss viscous dissipation. Shear production is small in barotropic conditions (i.e. when the horizontal pressure gradient is independent of height). Turbulent transport is an energy source.

Wyngaard (1983) estimated the Reynolds stress budget in convective boundary layers having substantial baroclinity and, hence, some measurable wind shear despite the strong convection. The budgets of lateral stress $\overline{u_2 u_3}$ and streamwise stress $\overline{u_1 u_3}$ were similar, being to lowest order a balance between shear production and pressure destruction. Turbulent

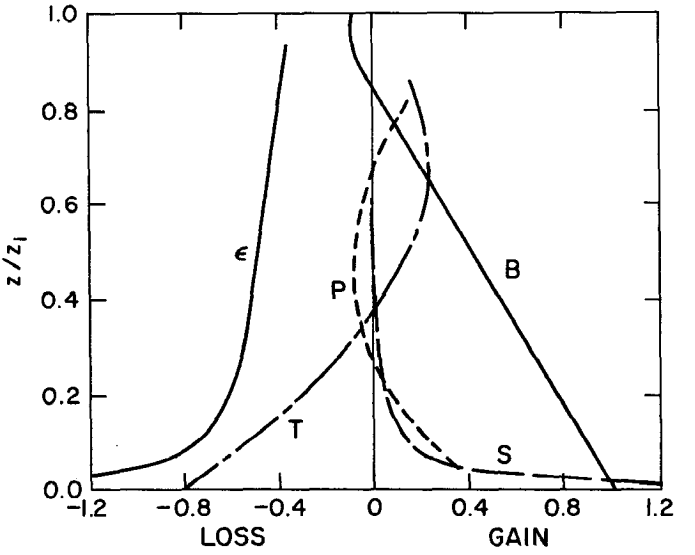

Figure 7 The budget of turbulent kinetic energy in the convective boundary layer, as summarized by Lenschow et al (1980). Symbols as in Figure 6.

transport and buoyant production were considerably smaller. To first approximation this is consistent with an eddy-viscosity relation

$$\overline{u_i u_3} = -K\frac{\partial U_i}{\partial x_3}, \qquad i = 1, 2, \tag{21}$$

with $K \sim 0.1\ w_* z_i$ in mid-layer. This is a result that should be tested through turbulence simulation (Section 7).

The budget of the vertical flux of temperature behaves quite differently in the mixed layer. Its principal gain term is turbulent transport, representing import from below; to first approximation this balances the loss to molecular destruction. The gradient production term varies from a small gain in the outer surface layer to near zero in mid mixed layer to a loss near the top, where the mean potential temperature gradient changes sign and the flux becomes counter-gradient. Thus, the eddy diffusivity for temperature has a mid-layer singularity, as pointed out by Deardorff (1966).

Moeng & Wyngaard (1984) used large-eddy simulation (LES) to study the top-down and bottom-up scalar flux budgets separately and found that the singularity occurs only in the bottom-up case; the top-down eddy diffusivity is quite well behaved. The budgets have other differences of detail, including a different time scale for the pressure destruction term in the two cases.

The different vertical transport properties for scalars released at the bottom and top of a convective boundary layer could be characteristic of convection driven from one side—in this case, the lower surface. A physical interpretation is that the uneven distribution of buoyant production (it is proportional to the temperature flux profile, which decreases linearly with height) imparts a distinct structure to the vertical velocity field throughout the layer: It has strong, relatively infrequent updrafts and weaker, more frequent downdrafts. The persistent buoyancy forces make the eddies coherent vertically, so the Lagrangian autocorrelation of vertical velocity acts for small times as if T_L is quite large—of the order of the large-eddy circulation time z_i/w_*. [In fact, T_L is formally zero because the flow is bounded in the vertical, so the autocorrelation changes sign at larger times (Tennekes & Lumley 1972).] This bimodal, time-coherent structure causes substantial differences in the transport of constituents released at the top and bottom of the layer.

Wyngaard & Weil (1991) suggested that transport asymmetry results from the interaction among the skewness of vertical velocity, its apparently large Lagrangian integral time scale, and a scalar flux gradient. They developed the simple constitutive equation

$$\overline{cw} = -K\frac{\partial C}{\partial z} - \frac{S(\overline{w^2})^{1/2}T_L}{2}\frac{\partial \overline{cw}}{\partial z}, \quad (22)$$

where $K \sim w_* z_i$ is a constant eddy diffusivity, $S = \overline{w^3}/(\overline{w^2})^{3/2}$ is the skewness of w, and T_L is the Lagrangian integral time scale. They showed that (22) qualitatively reproduces the LES results for scalar transport in the convective boundary layer.

Equations (21) and (22) suggest that convective turbulence has quite different transport properties for momentum and conservative scalar constituents. Perhaps this is related to the finding (Lesieur 1990) that a turbulent scalar field cascades more quickly to high wavenumbers than does the velocity field.

Moeng & Wyngaard (1989) used LES (Section 7) to study the behavior of the turbulent transport, pressure covariance, and dissipation terms in certain of the Reynolds equations for the convective boundary layer. They isolated the top-down and bottom-up diffusion processes and found that the transport terms behaved differently in the two cases, and not, in general, as gradient diffusion. They found that the pressure covariance in the scalar flux budget represented not only return-to-isotropy effects, as in (20), but also important buoyancy effects.

7. SIMULATING ATMOSPHERIC TURBULENCE

Given the difficulties and limitations of direct measurements of atmospheric turbulence, an attractive supplementary source of data is simulation—experimental, in laboratory flows, or numerical, on the computer.

Corrsin (1961) speculated on the role of "large computing machines" in turbulence research. After estimating that about 10^{12} grid points would be required for a calculation at adequately large Reynolds number, he wrote "The foregoing estimate is enough to suggest the use of analog instead of digital computation; in particular, how about an analog consisting of a tank of water?"

In the 1970s Deardorff and Willis began a series of experiments with water in a laboratory convection tank 1 m on a side, using a layer of less dense fluid at typically 20 cm above the heated surface to cap the convection. The turbulence structure they reported (Willis & Deardorff 1974, Deardorff & Willis 1985, 1987) bore a striking resemblance to that of the convective atmospheric boundary layer, despite its much lower Reynolds number (R_ℓ was about 4×10^3, four orders of magnitude less than in the atmosphere), the absence of mean shear, and the differences in geometry. This tank was also used to study the dispersion of turbulent plumes, both buoyant and nonbuoyant. Its results caused a major revamping of short-

range dispersion modeling in the lower atmosphere (Weil 1988, Briggs 1988).

Laboratory simulation is also used in studying transport and diffusion in stably stratified flows in complex terrain (Snyder 1985). In such applications it both enhances basic understanding of the phenomena and gives useful rules of thumb for applications. Turbulent entrainment across a density interface, an important problem in geophysical turbulence, has long been studied through laboratory simulation (Nokes 1988). The neutral boundary layer without stratification has been simulated in the laboratory by Caldwell et al (1972). Jayesh et al (1991) have studied stratified turbulence sandwiched between layers of neutral turbulence, which has relevance to the shear-free interfacial layer.

Over the past three decades there has been increasing interest in calculation methods for turbulent flows. I will separate the many ways in which one can attempt to calculate turbulence properties into two categories: modeling and simulation. In "modeling" one represents turbulence through approximate equations that display behavioral similarities to turbulence. In "simulation" one uses equations that are derivable from the exact set and, hence, remain faithful to the essential physics. While this distinction between modeling and simulation is not commonly accepted, I think it is useful.

In discussing second-order models of atmospheric turbulence, Lumley (1983) described a turbulence model as "a calibrated surrogate for turbulence." Regarding performance, he wrote "We would thus expect that the models would work satisfactorily in situations not too far removed geometrically, or in parameter values, from the benchmark situations used to calibrate the model."

It now seems generally, if implicitly, agreed that turbulence models are not predictive tools. It was not always so. Quoting Lumley again,

> Many of the initial successes of the models (in comparison to first order ones) have been in more complex flows, involving heat transfer, buoyancy and the like, because the relevant physical mechanisms are included. In addition, some of the successes have been in flows dominated by inertia or mean buoyancy, where the details of the turbulence model are irrelevant. Thus emboldened, the modelers have been overenthusiastic in promoting their models for other complex situations, often without considering at depth the difficult questions that arise. Consequently, there is some disillusionment with the models, a feeling that they embody too many *ad hoc* assumptions, and that they are unreliable as a result. . . . This reaction is probably justified, but it would be a shame if it resulted in a cessation of efforts to put a little more physics and mathematics into the models.

Turbulence models will probably always be important—even if the "turbulence problem" is solved. Zeman (1981) reviewed recent progress

in modeling planetary boundary layers, and pointed out areas where the models need improvement. I believe that at this time numerical simulation offers the best path to these improvements.

In large-eddy simulation only the largest eddies are simulated; those smaller than the grid are modeled. Since it is believed to be more important to treat the largest eddies reliably, I classify LES under simulation.

Moeng (1986, 1987), Mason & Thomson (1987), Nieuwstadt & de Valk (1987), Mason (1989), Schmidt & Schumann (1989), Sykes & Henn (1989), and Mason & Derbyshire (1990) have applied LES to atmospheric boundary-layer flows. Each uses a code that is broadly similar to that of Deardorff (1972), although there are differences in the spatial discretization (some use spectral techniques in the horizontal, some finite differences) and subgrid closures. Today's larger computers allow about 10^6 spatial grid points in PBL applications, making a $96 \times 96 \times 96$ grid, for example, quite feasible.

The difficulty of assembling suitable data bases on atmospheric turbulence (Section 3) makes definitive testing of atmospheric LES results difficult. Deardorff (1974), for example, could check only gross aspects of his simulation of Day 33 in the Wangara experiment against the observations. Moeng (1984) tested against an analytical Taylor-Green vortex flow and the Wangara data. Others have used laboratory data; Schumann and coworkers, for example, used the Adrian et al (1986) convection studies, and Mason (1989) and Nieuwstadt & de Valk (1987) used the Deardorff-Willis tank results. Figure 8 shows Moeng's LES results for the turbulence kinetic energy budget in the convective boundary layer and comparisons of various budget terms with laboratory and atmospheric measurements.

LES results are so detailed and complete that they can be immediately useful in modeling. For example, Ebert et al (1989) used LES results to obtain insight into Stull's (1984) closure for convective turbulence. Moeng & Wyngaard (1989) used it to assess the turbulent transport and dissipation-rate closures used in second-order models of the atmospheric boundary layer. Schumann (1989) used LES to study turbulent diffusion of reactive species in the convective boundary layer. Mason & Derbyshire (1990) reported the first LES studies of a stably stratified PBL and showed that the essence of certain previous models of it was correct. These studies demonstrate the potential of LES; it is doubtful that any of them could have been done through direct measurements in the atmosphere.

LES as applied to atmospheric turbulence has some limitations, including the subgrid-scale (SGS) closure and limited domain size. LES typically uses a variant of the Smagorinski (1963) model of the effects of eddies smaller than the numerical grid. Within the boundary layer the energy-

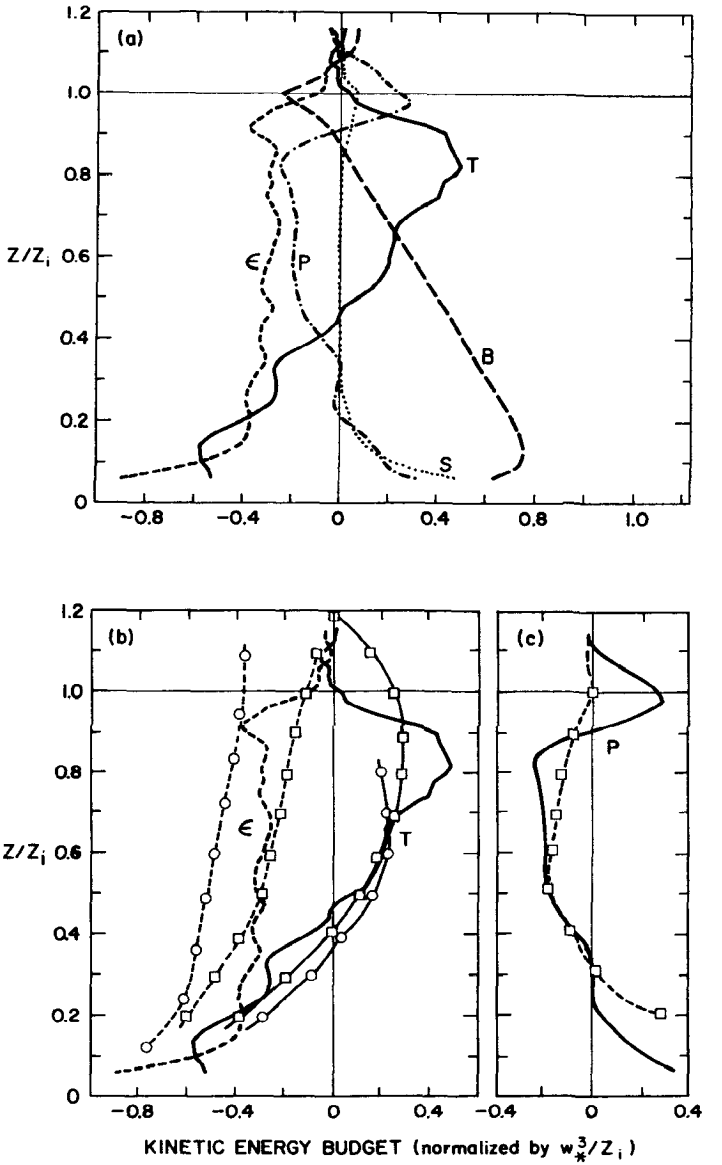

Figure 8 LES results for the turbulent kinetic energy budget in the convective boundary layer. Upper panel: complete budget, labels as in Figure 6. Note the overall agreement with the experimental results in Figure 7. Lower panel, left: comparisons of ε and T from LES with Deardorff-Willis (1985) tank results (*squares*) and Lenschow et al (1980) atmospheric results (*circles*). Lower right: comparison of P from LES with tank results. Figure courtesy of C.-H. Moeng, NCAR.

containing range is typically well resolved, with a negligible portion of the turbulent fluxes carried by the subgrid-scale eddies. Near the lower surface, however, this is not the case. Mason (personal communication) has found that existing subgrid-scale closures do not perform well there; the mean-field gradients, for example, are systematically larger than measured. He attributes this in part to the use of an ensemble-mean subgrid scheme that fails to account for the temporally and spatially local variations in the subgrid-scale flux divergences, or what is sometimes called "stochastic backscatter."

The subgrid schemes used today are independent of Reynolds number. Thus, it is not possible to use today's LES codes to investigate whether flow structure depends on Reynolds number.

The requirement that the energy-containing range be resolved restricts LES in boundary-layer applications to domains no larger than about 10 km in the horizontal. This limits its utility in problems involving surface variations; in many such cases one would like to be able to simulate domains perhaps an order of magnitude larger.

Direct numerical simulation (DNS)—which involves the numerical solution of the Navier-Stokes equations without closure assumptions—is having a huge impact on turbulence research (Hunt 1988, Reynolds 1990). It is limited to flows of low turbulence Reynolds number, since all eddies must be resolved, but with today's machines R_λ values in the range 50–100 are possible. Such simulations appear to be on the verge of yielding an inertial subrange (Kerr 1985). DNS is believed to be useful as a predictor of flows at larger Reynolds number because of the observation that above a threshold value, the energy-containing range structure of turbulent flows generally varies only weakly with Reynolds number.

DNS has only recently been applied to the atmospheric boundary layer. Coleman et al (1990b) presented results from the direct numerical simulation under neutral, unstable, and stable stratifications. The neutral runs showed that Coriolis forces do influence the turbulence; differences as large as 20% in the geostrophic drag coefficient and 70% in the angle between the freestream velocity and the surface shear stress were found. Longitudinal roll cells were found only under mildly unstable conditions; they carried about 10% of the heat and momentum fluxes. The stable results supported Nieuwstadt's (1984) local scaling scheme and other models, and agreed well with the Mason-Derbyshire (1990) LES results. The authors reported many instances in which their DNS results were very similar to those found through LES.

DNS cannot be used to represent the turbulent fine structure of the atmosphere, since that does depend on Reynolds number (Figure 1). One caveat on DNS of atmospheric turbulence, then, is that it is not trustworthy

in any problem that depends significantly on fine structure. Examples could include the role of turbulence in droplet coalescence processes in clouds (Tennekes & Woods 1973), and relative diffusion at small separations (Novikov 1989, Thomson 1990).

ACKNOWLEDGMENTS

The author is grateful to his colleagues A. Andrén, T. Horst, R. Kerr, D. H. Lenschow, J. McWilliams, C.-H. Moeng, and J. Weil for helpful comments during the preparation of this review.

Literature Cited

Adrian, R. J., Ferreira, R. T. D. S., Boberg, T. 1986. Turbulent thermal convection in wide horizontal fluid layers. *Exp. Fluids* 4: 121–41

Antonia, R. A., Anselmet, F., Chambers, A. J. 1986. Assessment of local isotropy using measurements in a turbulent plane jet. *J. Fluid Mech.* 163: 365–91

Andreas, E. L. 1987. On the Kolmogorov constants for the temperature-humidity cospectrum and the refractive index spectrum. *J. Atmos. Sci.* 44: 2399–2406

Atlas, D., Walter, B., Chou, S.-H., Sheu, P. J. 1986. The structure of the unstable marine boundary layer viewed by lidar and aircraft observations. *J. Atmos. Sci.* 43: 1301–18

Brasseur, J. G. 1991. Comments on the Kolmogorov hypothesis of isotropy in the small scales. *AIAA-91-0230, 29th Aerospace Sciences Meeting*, January, 1991, Reno

Briggs, G. 1988. Analysis of diffusion field experiments. In *Lectures on Air Pollution Modeling*, ed. A. Venkatram, J. Wyngaard, pp. 63–117. Boston: Amer. Meteor. Soc. 390 pp.

Brost, R. A., Wyngaard, J. C., Lenschow, D. H. 1982. Marine stratocumulus layers. Part II: Turbulence budgets. *J. Atmos. Sci.* 38: 818–36

Brutsaert, W., Sugith, M. 1990. The extent of the unstable Monin-Obukhov layer for temperature and humidity above complex hilly grassland. *Boundary-Layer Meteorol.* 51: 383–400

Caldwell, D. R., Van Atta, C. W., Helland, K. N. 1972. A laboratory study of the turbulent Ekman layer. *Geophys. Fluid Dyn.* 3: 125–60

Caughey, S. J., Wyngaard, J. C. 1979. The turbulent kinetic energy budget in convective conditions. *Q. J. R. Meteorol. Soc.* 105: 231–39

Caughey, S. J., Wyngaard, J. C., Kaimal, J. C. 1979. Turbulence in the evolving stable boundary layer. *J. Atmos. Sci.* 36: 1041–52

Caughey, S. J. 1982. Observed characteristics of the atmospheric boundary layer. In *Atmospheric Turbulence and Air Pollution Modelling*, ed. F. T. M. Nieuwstadt, H. van Dop, pp. 107–58. Dordrecht: Reidel. 358 pp.

Champagne, F. 1978. The fine-scale structure of the turbulent velocity field. *J. Fluid Mech.* 86: 67–108

Champagne, F. H., Friehe, C. A., LaRue, J. C., Wyngaard, J. C. 1977. Flux measurements, flux estimation techniques, and fine-scale turbulence measurements in the unstable surface layer over land. *J. Atmos. Sci.* 34: 515–30

Chen, C., Cotton, W. R. 1987. The physics of the marine stratocumulus-capped mixed layer. *J. Atmos. Sci.* 44: 2951–77

Chou, S.-H., Yeh, E.-N. 1987. Airborne measurements of surface layer turbulence over the ocean during cold air outbreaks. *J. Atmos. Sci.* 44: 3721–33

Coleman, G. N., Ferziger, J. H., Spalart, P. R. 1990a. A numerical study of the turbulent Ekman layer. *J. Fluid Mech.* 213: 313–48

Coleman, G. N., Ferziger, J. H., Spalart, P. R. 1990b. A numerical study of the stratified turbulent Ekman layer. *Report No. TF-48*, Dept. Mech. Eng., Stanford Univ., Stanford, CA. 245 pp.

Corrsin, S. 1951. On the spectrum of isotropic temperature fluctuations in isotropic turbulence. *J. Appl. Phys.* 22: 469–73

Corrsin, S. 1961. Turbulent flow. *Am. Sci.* 49: 300–25

Corrsin, S. 1963. Turbulence: Experimental methods. *Handb. Phys.* Stromungsmechanik II, VIII/2: 524–90. Berlin: Springer-Verlag

Curry, J. A., Ebert, E. E., Herman, G. F. 1988. Mean and turbulence structure of the summertime Arctic cloudy boundary layer. *Q. J. R. Meteorol. Soc.* 114: 715–46

Deardorff, J. W. 1966. The counter-gradient heat flux in the atmosphere and in the laboratory. *J. Atmos. Sci.* 23: 503–6

Deardorff, J. W. 1970. Convective velocity and temperature scales for the unstable planetary boundary layer and for Rayleigh convection. *J. Atmos. Sci.* 27: 1211–13

Deardorff, J. W. 1972. Numerical investigation of neutral and unstable planetary boundary layers. *J. Atmos. Sci.* 29: 91–115

Deardorff, J. W. 1973. An explanation of anomalously large Reynolds stresses within the convective planetary boundary layer. *J. Atmos. Sci.* 30: 1070–76

Deardorff, J. W. 1974. Three dimensional numerical study of the height and mean structure of an entraining mixed layer. *Boundary-Layer Meteorol.* 7: 81–106

Deardorff, J. W. 1979. Prediction of convective mixed-layer entrainment for realistic capping inversion structure. *J. Atmos. Sci.* 36: 424–36

Deardorff, J. W. 1980. Stratocumulus-capped mixed layers derived from a three-dimensional model. *Boundary-Layer Meteorol.* 18: 495–527

Deardorff, J. W., Willis, G. E. 1985. Further results from a laboratory model of the convective planetary boundary layer. *Boundary-Layer Meteorol.* 32: 205–36

Deardorff, J. W., Willis, G. E. 1987. Turbulence within a baroclinic laboratory mixed layer above a sloping surface. *J. Atmos Sci.* 44: 772–78

Derbyshire, S. H. 1990. Nieuwstadt's stable boundary layer revisited. *Q. J. R. Meteorol. Soc.* 116: 127–58

Dobson, F. W. 1980. Air pressure measurement techniques. In *Air-Sea Interaction: Instruments and Methods*, ed. F. Dobson, L. Hasse, R. Davis, pp. 231–54. New York: Plenum. 801 pp.

Duynkerke, P. G., Driedonks, A. G. M. 1987. A model for the turbulent structure of the stratocumulus-topped atmospheric boundary layer. *J. Atmos. Sci.* 44: 43–64

Duynkerke, P. G., Driedonks, A. G. M. 1988. Turbulent structure of a shear-driven stratus-topped atmospheric boundary layer: A comparison of model results with observations. *J. Atmos. Sci.* 45: 2343–51

Ebert, E. E., Schumann, U., Stull, R. B. 1989. Nonlocal turbulent mixing in the convective boundary layer evaluated from large-eddy simulation. *J. Atmos. Sci.* 46: 2178–2207

Fairall, C. W. 1987. A top-down and bottom-up diffusion model of C_T^2 and C_Q^2 in the entraining convective boundary layer. *J. Atmos. Sci.* 44: 1009–17

Frisch, A. S., Martner, B. E., Gibson, J. S. 1989. Measurement of the vertical flux of turbulent kinetic energy with a single Doppler radar. *Boundary-Layer Meteorol.* 49: 331–37

Hanson, H. P. 1987. Radiative/turbulent transfer interactions in clouds. *J. Atmos. Sci.* 44: 1287–95

Hill, R. J. 1978a. Models of the scalar spectrum for turbulent advection. *J. Fluid Mech.* 88: 541–62

Hill, R. J. 1978b. Spectra of fluctuations in refractivity, temperature, humidity, and the temperature-humidity cospectrum in the inertial and dissipative ranges. *Radio Sci.* 13: 953–61

Hill, R. J. 1989. Implications of Monin-Obukhov similarity theory for scalar quantities. *J. Atmos. Sci.* 46: 2236–44

Hogstrom, U. 1990. Analysis of turbulence structure in the surface layer with a modified similarity formulation for near neutral conditions. *J. Atmos. Sci.* 47: 1949–72

Hunt, J. C. R. 1981. Some connections between fluid mechanics and the solving of industrial and environmental fluid-flow problems. *J. Fluid Mech.* 106: 103–30

Hunt, J. C. R. 1988. Studying turbulence through direct numerical simulation: 1987 Center for Turbulence Research NASA Ames/Stanford Summer Programme. *J. Fluid Mech.* 190: 375–92

Hunt, J. C. R., Kaimal, J. C., Gaynor, J. E. 1988. Eddy structure in the convective boundary layer—new measurements and new concepts. *Q. J. R. Meteorol. Soc.* 114: 827–58

Huyuh, B. P., Coulman, C. E., Turner, T. R. 1990. Some turbulence characteristics of convectively mixed layers over rugged and homogeneous terrain. *Boundary-Layer Meteorol.* 51: 229–54

Jayesh, Yoon, K., Warhaft, Z. 1991. Turbulent mixing and transport in a thermally stratified layer formed in decaying turbulence. *Phys. Fluids A* 3: 1143–55

Kader, B. A., Yaglom, A. M. 1990. Mean fields and fluctuation moments in unstably stratified turbulent boundary layers. *J. Fluid Mech.* 212: 637–62

Kaimal, J. C., Wyngaard, J. C., Izumi, Y., Coté, O. R. 1972. Spectral characteristics of surface-layer turbulence. *Q. J. R. Meteorol. Soc.* 98: 563–89

Kaimal, J. C., Wyngaard, J. C., Haugen, D. A., Coté, O. R., Izumi, Y., Caughey, S. J., Readings, C. J. 1976. Turbulence structure in the convective boundary layer. *J. Atmos. Sci.* 33: 2152–69

Kerr, R. M. 1985. Higher-order derivative correlations and the alignment of small-scale structures in isotropic numerical turbulence. *J. Fluid Mech.* 153: 31–58
Kristensen, L., Lenschow, D. H., Kirkegaard, P., Courtney, M. 1989. The spectral velocity tensor for homogeneous boundary layer turbulence. *Boundary-Layer Meteorol.* 47: 149–93
Kustas, W. P., Brutsaert, W. 1987. Budgets of water vapor in the unstable boundary layer over rugged terrain. *J. Clim. Appl. Meteorol.* 26: 607–20
Lenschow, D. H. 1979. Model of the height variation of the turbulent kinetic energy budget in the planetary boundary layer. *J. Atmos. Sci.* 31: 465–74
Lenschow, D. H., Wyngaard, J. C., Pennell, W. T. 1980. Mean-field and second-moment budgets in a baroclinic, convective boundary layer. *J. Atmos. Sci.* 37: 1313–26
Lenschow, D. H., Stankov, B. B. 1986. Length scales in the convective boundary layer. *J. Atmos. Sci.* 43: 1198–1209
Lenschow, D. H., Li, X. S., Zhu, C. J., Stankov, B. B. 1988. The stably stratified boundary layer over the Great Plains. 1. Mean and turbulence structure. *Boundary-Layer Meteorol.* 42: 95–122
Lesieur, M. 1990. The utility and drawbacks of traditional approaches: Comment 2. In *Whither Turbulence?*, ed. J. Lumley, *Lecture Notes in Physics* 357: 59–69. Berlin: Springer-Verlag. 535 pp.
Lewellen, W. S., Teske, M. E. 1973. Prediction of the Monin-Obukhov similarity functions from an invariant model of turbulence. *J. Atmos. Sci.* 30: 1340–45
Lilly, D. K. 1968. Models of cloud-topped mixed layers under a strong inversion. *Q. J. R. Meteorol. Soc.* 94: 292–309
Lumley, J. L. 1983. Atmospheric modelling. *Mech. Eng. Trans.*, Inst. Eng., Australia. ME8: 153–59
Lumley, J. L., Panofsky, H. A. 1964. *The Structure of Atmospheric Turbulence*. New York: Interscience. 239 pp.
Mahrt, L. 1989. Intermittency of atmospheric turbulence. *J. Atmos. Sci.* 46: 79–95
Mahrt, L., Gamage, N. 1987. Observations of turbulence in stratified flow. *J. Atmos. Sci.* 44: 1106–21
Mason, P. J. 1989. Large eddy simulation of the convective atmospheric boundary layer. *J. Atmos. Sci.* 46: 1492–1516
Mason, P. J., Thomson, D. J. 1987. Large-eddy simulation of the neutral-static-stability planetary boundary layer. *Q. J. R. Meteorol. Soc.* 113: 413–43
Mason, P. J., Derbyshire, S. H. 1990. Large-eddy simulation of the stably stratified atmospheric boundary layer. *Boundary-Layer Meteorol.* 53: 117–62
McBean, G. A., Elliot, J. A. 1975. The vertical transport of kinetic energy by turbulence and pressure in the boundary layer. *J. Atmos. Sci.* 32: 753–66
Mellor, G. L. 1973. Analytic prediction of the properties of stratified planetary surface layers. *J. Atmos. Sci.* 30: 1061–69
Moeng, C.-H. 1984. A large-eddy-simulation model for the study of planetary boundary layer turbulence. *J. Atmos. Sci.* 41: 2052–62
Moeng, C.-H. 1986. Large-eddy simulation of a stratus-topped boundary layer. Part I: Structure and budgets. *J. Atmos. Sci.* 43: 2886–2900
Moeng, C.-H. 1987. Large-eddy simulation of a stratus-topped boundary layer. Part II: Implications for mixed-layer modeling. *J. Atmos. Sci.* 44: 1605–14
Moeng, C.-H., Wyngaard, J. C. 1984. Statistics of conservative scalars in the convective boundary layer. *J. Atmos. Sci.* 41: 3161–69
Moeng, C.-H., Wyngaard, J. C. 1989. Evaluation of turbulent transport and dissipation closures in second-order modeling. *J. Atmos. Sci.* 46: 2311–30
Nieuwstadt, F. T. M. 1984. The turbulent structure of the stable nocturnal boundary layer. *J. Atmos. Sci.* 41: 2202–16
Nieuwstadt, F. T. M., de Valk, J. P. J. M. M. 1987. A large-eddy simulation of buoyant and non-buoyant plume dispersion in the atmospheric boundary layer. *Atmos. Environ.* 21: 2573–81
Nokes, R. I. 1988. On the entrainment rate across a density interface. *J. Fluid Mech.* 188: 185–204
Novikov, E. 1989. Two-particle description of turbulence, Markov property, and intermittency. *Phys. Fluids A* 1: 326–30
Panofsky, H. A., Dutton, J. A. 1984. *Atmospheric Turbulence*. New York: Wiley. 397 pp.
Reynolds, W. C. 1990. The potential and limitations of direct and large eddy simulations. In *Whither Turbulence?*, ed. J. Lumley, *Lecture Notes in Physics* 357: 313–43. Berlin: Springer-Verlag. 535 pp.
Rotta, J. C. 1951. Statistische theorie nichthomogener turbulenz. *Z. Phys.* 129: 547–72
Schmidt, H., Schumann, U. 1989. Coherent structure of the convective boundary layer deduced from large-eddy simulation. *J. Fluid Mech.* 200: 511–62
Schumann, U. 1989. Large-eddy simulation of turbulent diffusion with chemical reactions in the convective boundary layer. *Atmos. Environ.* 23: 1713–27

Scorer, R. S. 1980. Book review. *Clean Air* 10: 148–49
Smagorinski, J. 1963. General circulation experiments with the primitive equations. I. The basic experiment. *Mon. Weather Rev.* 91: 99–164
Snyder, W. H. 1985. Fluid modeling of pollutant transport and diffusion in stably stratified flows over complex terrain. *Annu. Rev. Fluid Mech.* 17: 239–66
Stull, R. B. 1984. Transient turbulence theory. Part I: The concept of eddy-mixing across finite distances. *J. Atmos. Sci.* 41: 3351–67
Sykes, R. I., Henn, D. S. 1989. Large-eddy simulation of turbulent sheared convection. *J. Atmos. Sci.* 46: 1106–18
Tennekes, H. 1970. Free convection in the turbulent Ekman layer of the atmosphere. *J. Atmos. Sci.* 27: 1027–34
Tennekes, H. 1975. A model for the dynamics of the inversion above a convective boundary layer. *J. Atmos. Sci.* 32: 558–67
Tennekes, H. 1978. Turbulent flow in two and three dimensions. *Bull. Am. Meteorol. Soc.* 59: 22–28
Tennekes, H., Lumley, J. L. 1972. *A First Course in Turbulence*. Cambridge: MIT Press. 300 pp.
Tennekes, H., Woods, J. D. 1973. Coalescence in a weakly turbulent cloud. *Q. J. R. Meteorol. Soc.* 99: 758–63
Tennekes, H., Driedonks, A. G. M. 1981. Basic entrainment equations for the atmospheric boundary layer. *Boundary-Layer Meteorol.* 20: 515–31
Thomson, D. J. 1990. A stochastic model for the motion of particle pairs in isotropic high-Reynolds-number turbulence, and its application to the problem of concentration variance. *J. Fluid Mech.* 210: 113–53
Van der Hoven, I. 1957. Power spectrum of horizontal wind speed in the frequency range from 0.0007 to 900 cycles per hour. *J. Meteorol.* 14: 160–64
Weil, J. C. 1985. Updating applied diffusion models. *J. Clim. Appl. Meteorol.* 24: 1111–30
Weil, J. C. 1988. Atmospheric dispersion—Observations and models. In *Flow and Transport in the Natural Environment: Advances and Applications*, ed. W. Steffen, O. Denmead, pp. 352–76. Berlin: Springer-Verlag. 384 pp.
Wieringa, J. 1980. A revaluation of the Kansas mast influence on measurements of stress and cup anemometer overspeeding. *Boundary-Layer Meteorol.* 18: 411–30
Willis, G. E., Deardorff, J. W. 1974. A laboratory model of the unstable planetary boundary layer. *J. Atmos. Sci.* 31: 1297–1307
Wucknitz, J. 1980. Flow distortion by supporting structures. In *Air-Sea Interaction, Instruments and Methods*, ed. F. Dobson, L. Hasse, pp. 605–26. Plenum. 815 pp.
Wyngaard, J. C. 1973. On surface-layer turbulence. In *Workshop on Micrometeorology*, ed. D. Haugen, pp. 101–49. Boston: Am. Meteorol. Soc. 392 pp.
Wyngaard, J. C. 1983. The mean wind structure of the baroclinic, convective boundary layer. In *Mountain Meteorology*, ed. E. Reiter, Z. Baozhen, Q. Yongfu, pp. 371–96. Beijing: Science Press. 699 pp.
Wyngaard, J. C. 1988. The effects of probe-induced flow distortion on atmospheric turbulence measurements: Extension to scalars. *J. Atmos. Sci.* 45: 3400–12
Wyngaard, J. C., Coté, O. R., Izumi, Y. 1971. Local free convection, similarity, and the budgets of shear stress and heat flux. *J. Atmos. Sci.* 28: 1171–82
Wyngaard, J. C., Businger, J. A., Kaimal, J. C., Larsen, S. E. 1982. Comments on "A revaluation of the Kansas mast influence on measurements of stress and cup anemometer overspeeding." *Boundary-Layer Meteorol.* 22: 245–50
Wyngaard, J. C., Brost, R. A. 1984. Top-down and bottom-up diffusion of a scalar in the convective boundary layer. *J. Atmos. Sci.* 41: 102–12
Wyngaard, J. C., Rockwell, L., Friehe, C. A. 1985. Errors in the measurement of turbulence upstream of an axisymmetric body. *J. Atmos. Ocean. Tech.* 2: 605–14
Wyngaard, J. C., Weil, J. C. 1991. Transport asymmetry in skewed turbulence. *Phys. Fluids A* 3: 155–62
Yaglom, A. M. 1977. Comments on wind and temperature flux-profile relationships. *Boundary-Layer Meteorol.* 11: 89–102
Young, G. S. 1987. Mixed layer spectra from aircraft measurements. *J. Atmos. Sci.* 44: 1251–56
Zeman, O. 1981. Progress in the modeling of planetary boundary layers. *Annu. Rev. Fluid Mech.* 13: 253–72
Zilitinkevich, S. S. 1975. Comments on "A model for the dynamics of the inversion above a convective boundary layer." *J. Atmos. Sci.* 32: 991–92

Annual Review of Fluid Mechanics
Volume 24, 1992

CONTENTS